

# **Linear viscoelastic models**

## **Part IV. From molecular dynamics to temperature and viscoelastic relations using control theory**

Tommi Borg<sup>1</sup>

*TomCoat Oy, Koskisenkuja 11, 62500 Evijärvi, Finland*

Esko J. Pääkkönen

*Tampere University of Technology, Laboratory of Plastics and Elastomer Technology,  
P.O. Box 589, 33101 Tampere, Finland*

Viscoelasticity and temperature dependences are explained using molecular dynamics and control theory. We have previously [1–3] applied control theory to model the relationship between the relaxation modulus, dynamic and shear viscosity, transient flow effects, power law and Cox-Merz rule related to the molecular weight distribution (MWD), and here these topics are discussed more generally. In this paper we show the direct simple relation to molecular dynamics using structural models comprising dumb-bells [4] with internal viscosity and elasticity in a statistical tube. The dumb-bell model is used to obtain the linear relation to the elasticity  $P'$  value of function  $P'(\omega)$  and the relation to the viscosity  $P''$  value of function  $P''(\omega)$  from chain friction. The applied principle is also valid for the relaxation modulus or shear viscosity. A new principle is presented for obtaining absolute values such as zero viscosity by modelling, which is first used to obtain absolute values for a target point at a high rate for unentangled chains (since close relaxed states of chain topology are much more complicated). An analytical model for the temperature dependency of viscoelastic flows is presented, which is many times more accurate than WLF or Arrhenius equations. Control theory and variations of

---

<sup>1</sup> To whom correspondence should be addressed.

tube diameter as a function of temperature gives linear relation between chain dynamics and viscoelastic properties. New compact formulas are presented to simultaneously model different polymer flows and temperatures. We have also found that the MWDs computed from the relaxation modulus or complex and the shear viscosity are not temperature sensitive, in contrast to what time–temperature superposition (TTS) suggests, although absolute viscoelastic values make them appear very temperature dependent. TTS is verified for thermorheologically simple materials, and the reasons for it not holding are explained.

*Keywords:* Molecular dynamics, Control theory, Temperature dependence, TTS, Polydispersity.

## **1. Introduction**

As we reported previously [1–3], control theory can be used to precisely model viscoelastic flows accurately at a constant temperature. The next natural question is whether this control theory schema can be used for modelling relations to chain dynamics and as a function of temperature.

Molecular dynamics related to different flows and control theory formulas was modelled in the present study. We obtained simple linear relationships consistent with all of our previous findings. We also obtained an analytical model for the temperature dependence as a rheologically effective distribution (RED) for temperature ( $RED^T$ ), which is actually related to the thermal expansion curve and tube diameter as a function of temperature, which is essential in our model for dynamic chains based on the dumb-bell model [4] and friction.

Our previous studies revealed the great puzzle that the molecular weight distribution (MWD) or the respective RED computed from the relaxation modulus or complex and shear

viscosity is not temperature sensitive, although these curves are clearly strongly temperature-dependent. Fig. 1 shows that the curves of relaxation modulus  $G(t)$  and complex viscosity  $\eta^*(\omega)$  at 250°C and 130°C are totally different, but the related elastic REDs (RED's) have minimal differences. Different curves were generated using elastic  $P'$  and viscous  $P''$  constants and deviation in zero viscosity  $\eta_0$  and modulus  $G_0$ . The figure shows only the foremost distributions, and frequency  $\log \omega$  approximately varies according to 0.13%/1°C on a logarithmic scale.

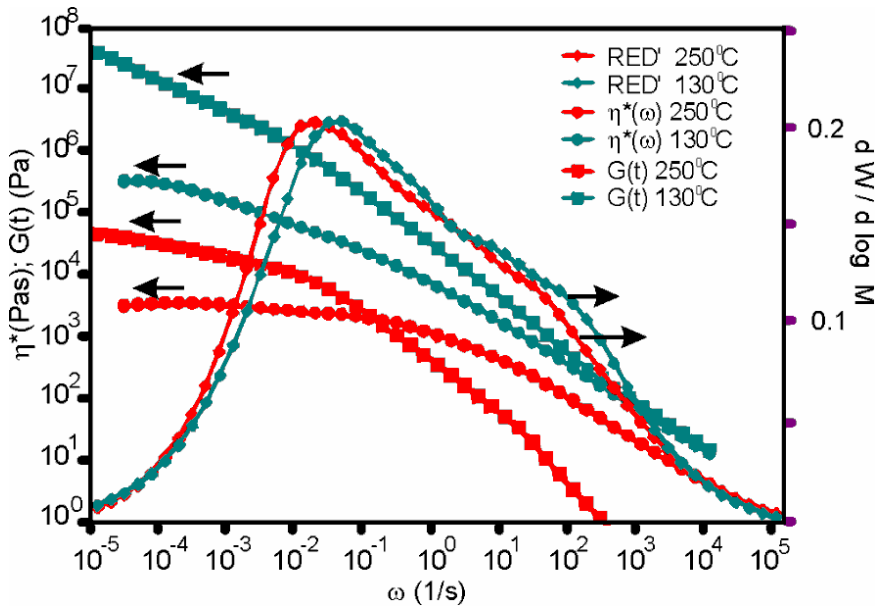


**Figure 1.** Chart visualizes the puzzle that the elastic RED' and its related MWD computed by melt calibration are not temperature sensitive, whereas the shown foremost RED's at 250°C and 130°C are linearly related to  $G(t)$  and  $\eta * (\omega)$  at their respective temperatures.

The above puzzle conflicts with many previous studies on rheology and time-temperature superposition (TTS), whereas similar types of results have been obtained by van Gurp and Palmen [5] and many other authors [6–12]. However, since our results obtained using precise models were more reliable than those developed previously, we were able to investigate this anomaly and verify TTS only for thermorheologically simple materials.

We developed compact and analytical formulas using a principle similar to that used in our previous studies. Some measurements at different temperatures, new computations, and the respective WLF and Arrhenius equations are compared, which revealed that the new model introduced in this study is four times more precise than the previous models.

## 2. Theory

### 2.1. Relations to molecular dynamics

Molecular dynamics related to different flows modelled using control theory is discussed. A relaxation-time schema is a good starting point for rough estimations of viscoelasticity. We can approximate relaxation times or generate the entire relaxation spectrum, but if a single relaxation time does not accurately describe the rheology on a macro scale, how would a tube equilibration time  $\tau_e$  or disengagement time  $\tau_d$  work better on a molecular scale? According to this consideration, we used the dumb-bell model in a statistical tube.

A further development from a simple linear elastic (Hookean) dumb-bell model is the finitely extensible non-linear elastic (FENE) dumb-bell model [4] that describes three-dimensional flows using the Fokker-Planck equation, yielding a distribution function. An alternative is to use a stochastic approach with the Fokker-Planck equation and the Itô stochastic differential equation [13–15]. Also other micro-macro methods for multiscale simulations of viscoelastic flow using molecular models of kinetic theory have been discussed in the wide-ranging review by Keunings [16]. In our studies, we have converted these micro-level stochastic processes to the statistical micro-macro scale distributions of elastic  $P'(\omega)$  and viscous  $P''(\omega)$  functions, as is discussed below.

Viscosity and other friction-dependent properties such as self-diffusion can be modelled indirectly using the free-volume theory with the Doolittle formula. Another approach is to use the non-equilibrium Brownian dynamics of Hookean and FENE dumb-bells with internal viscosity, as discussed by Hua and Schieber [17], where internal viscosity is a non-inertial dumb-bell utilizing friction points with Stokes law for drag force and Brownian forces. As a starting formula obtained from the *modified Stokes law* [18] for the viscosity and restricting force, we use  $F'' = 6\pi\xi R\dot{x}$ , where  $\dot{x}$  is a general rate and  $\xi$  is the friction coefficient.

Many studies have investigated relaxed and entangled chains, but few have investigated shear-oriented molecules. We show an alternative physics-based procedure using an oriented chain structure and structural models with the dumb-bell analogy for the chain dynamics in a statistical tube.

In our previous study (see Part III, Eqs. (14) and (15) [3]), we partitioned the complex viscosity formula into dynamic moduli components  $G'$  and  $G''$ , where the analytical model for viscosity  $\eta^*(\omega) = \eta_0^* e^{-P'(\omega) - P''(\omega)}$  has elastic function  $P'(\omega)$  of the following form:

$$P'(\omega) = P' \int_{-\infty}^{\log \omega} w(\log \psi) \left( \log \frac{\omega}{\psi} \right) d \log \psi \quad (1)$$

Elasticity value  $P'$  (or actually the inverse value  $1/P'$  for elasticity, as shown below) can be explained by molecular dynamics using a simple modified elastic dumb-bell model. We start from the original model [4], where  $F_c$  is the force in one dimension exerted by the connector on the particle. The elastic force for a single chain is  $F_c = \frac{3kT}{\langle R^2 \rangle_0} x$ . Since the novel mean-square end-to-end distance in equilibrium  $\langle R^2 \rangle_0$  can lead to complicated treatments close relaxed states, we used an alternative presentation for the spring constant ( $K = \frac{3kT}{\langle R^2 \rangle_0}$ ) at an oriented steady high flow in the absence of chain entanglements.

Before writing linear relations for Eq. (1) for the elastic connector force  $F' = Kx$ , the original form of viscoelastic formulas [1–3] written in simplified form with elastic component  $\eta = e^{-P'(\omega)} = e^{-P'} e^{f(\cdot)} = \frac{1}{e^{P'}} e^{f(\cdot)}$  needs to be considered. Thus, we can write linear relations for elastic force  $F' = Kx \propto \frac{f(\cdot)}{P'}$ , where the integral  $f(\cdot)$  yields the displacement state  $x$  of chains compared with fully relaxed molecules. This integral of course relates also to the amount of entanglement and other chain dynamics. A value of  $x$  close to zero indicates a high degree of entanglement, while for a fully oriented state  $x$  is 1.

Since different definitions of the “tube diameter” and chain lengths are used in the literature, to avoid confusion we use here the *statistical radial tube diameter* ( $D_s$ ) and the *statistical unit segment length* ( $L_s$ ), as illustrated in Fig. 2a. The ratio  $L_s/D_s$  relates to spring constant  $K$ , since a larger tube diameter  $D_s$  produces a smaller  $K$  due to the chains being able to relax more in the radial direction and thereby reduce the stress along the backbone inside the tube. Backbones can have several degrees of rotational freedom in their bonds with different potential energies. If tube diameter  $D_s$  is small, backbones have fewer degrees of freedom, which can increase the stress along the tube for the same strain, resulting in a greater spring constant  $K$ . If we include the time influence, the relaxation process takes longer for a small tube of smaller diameter at a lower temperature.

We obtain elastic function  $P'(\omega)$  of Eq. (1) or product  $1/P' \cdot f(\cdot) = kKx$ , where scaling factor  $k$  includes all the effective molecules of distribution  $w(\log M)$  and the integral relates to the respective displacement state  $x$ . Thus, we obtain a simple formula for elasticity and inverse elasticity value  $1/P'$  using a statistically scaled spring constant  $k_s = kK$ :

$$1/P' = k_s \frac{L_s}{D_s} \quad (2)$$

We add temperature coefficient  $a'_T$  to Eq. (2) to model changes at different temperatures. The values of  $k'=1/k_s$  and  $a'_T$  differ between analytical and characteristic models due to differences in the values of  $P'$  and formula structures. Increasing temperature expands the tube diameter (increasing  $D_s$ ) and respectively decreases the inverse value  $1/P'$ , producing a corresponding  $P'$  increase in Eq. (3). If the polymer has branches, statistical unit segment length  $L_s$  increases (or  $D_s$  decreases) relatively for a unit backbone, elasticity value  $P'$  increases and inverse value  $1/P'$  decreases in Eq. (3) during a temperature increase, as obtained in practice for chains of the same chemical type:

$$P' = k' \frac{D_s}{L_s} + a'_T(T - T_0) \quad (3)$$

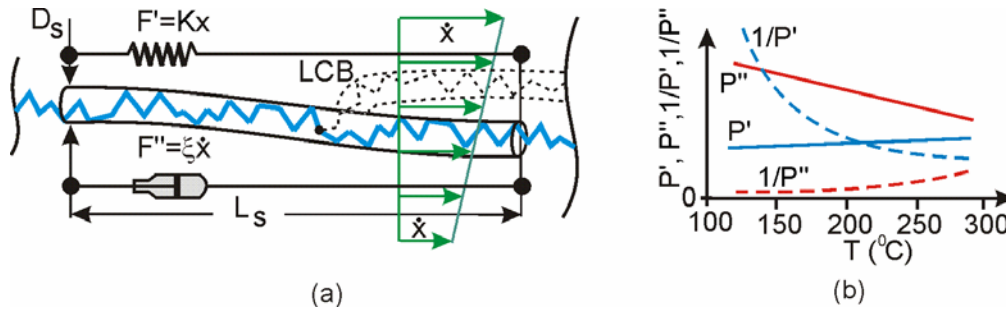


**Figure 2.** Dimensions of an oriented unit segment in a tube and graph of  $P'$  and  $P''$  values at different temperatures.

- a. Oriented unit segment at high shear drawn with roughly scaled dimensions used for modelling in Section 3. Possible long chain branching (LCB) increases statistical unit segment length  $L_s$ , and increasing temperature expands tube diameter  $D_s$ .
- b. Behaviours of  $P'$  and  $P''$  values and their inverse values are related directly to the elasticity ( $1/P'$ ) and viscosity ( $1/P''$ ) of the polymer.

For viscosity value  $P''$  we can start from internal viscous restricting force for a statistical unit segment  $F'' = \xi \dot{x} \propto P''(\omega)$ , where  $\xi$  is the internal friction coefficient between chains. A

higher temperature increases tube diameter  $D_s$  and internal friction coefficient  $\zeta$  decreases, making it easier for chains to flow at a lower viscous restricting force. We now construct a relation similar to  $L_s/D_s$  related to the friction and viscosity forces of the formula  $1/P'' \int() = k\xi\dot{x}$ . Thus, at a higher temperature inverse viscosity value  $1/P''$  increases and  $P''$  decreases. We obtain the formula for the relationship between  $a''_T$  and viscosity value  $P''$  shown in Eq. (4) as

$$P'' = k'' \frac{D_s}{L_s} + a''_T(T - T_0) \quad (4)$$

The above principle applies to the complex viscosity, but the procedure is also valid for relaxation modulus or shear viscosity. In the characteristic model,  $P'$  and  $P''$  have smaller values due to the algebraic structure of functions  $P'(\omega)$  and  $P''(\omega)$ .  $P'$  and  $P''$  values could also influence each other, but this was not investigated. In summary, from the original standpoint of molecular dynamics, the viscoelastic model should use the inverse values for  $P'$  and  $P''$ ; but, as shown below and illustrated in Fig. 2b, the presented form is even graphically linear when modelling  $P'$  and  $P''$  and is better for the practical modelling of viscoelasticity.

The next task is to find zero viscosity  $\eta_0$  from molecular dynamics, from which it is possible further to compute zero modulus, as showed in our previous studies [1–3]. Applying the Rouse-Bueche model for unentangled melt polymers [19] yields

$$\eta_0 = \frac{b^2 M \xi \rho N_A}{36 M_0^2} \quad (5)$$

where  $N_A$  is Avogadro's number and  $M_0$  is the molecular weight of the monomer ( $M/N$ ).

Eq. (5) applies only for unentangled chains, chain topology with the close relaxed state of an entangled molecule is the most complicated, and the possibility of long chain branches and other chain structures add complexity that generates variation in  $\eta_0$ . Measurements made in different studies [20–24] indicate that after reaching plateau modulus  $G_N^0$  at higher frequencies at

$\omega > 100/\text{s}$ , complex modulus  $G^*(\omega)$  or viscosity  $\eta^*(\omega)$  and  $\eta$  values approach each other for different molecular weights.

Thus, we use critical limit rate  $\omega_\infty$  and the respective limit complex modulus  $G_\infty^*$  or viscosity  $\eta_\infty^*$ , where all chains are oriented and unentangled. Applying the  $\omega_\infty$  to the integral of RED' does not further influence the response to the normalized limit value 1. This critical limit frequency for the example shown in Fig. 1 is  $\omega_\infty = 10^5/\text{s}$ , where the  $M$  or  $w(M)$  RED' no longer has an influence. Thus, we can write Eq. (5) for critical limit complex viscosity  $\eta_\infty^*$  as follows:

$$\eta_\infty^* = \frac{L_s^2 \xi \rho N_A}{36 M_0} \quad (6)$$

This point is normally outside the measurement range, but does not generate difficulties for software and the principle has already been used for years in practice, with these  $\eta_\infty^*(\omega_\infty)$  absolute target points for viscosity found in practice depending only on the used polymer chemical structure and temperature. The MWD can be used to compute zero viscosity  $\eta_0^*$  and also zero modulus  $G_0$ , as shown in our previous studies. Again the above procedure is valid also for shear viscosity  $\eta$ .

## 2.2. Temperature dependence modelled using control theory

We first use control theory to generate absolute values for zero viscosity  $\eta_0^*(T)$  and as a function of temperature, and then use complete formulas at different frequencies or as a function of time. We use a procedure similar to that used in our previous studies to directly obtain the analytical formula for zero viscosity by using RED<sup>T</sup>  $w(\log T)$  and temperature value  $P^T$ :

$$\log \frac{\eta_0^*(T)}{\eta_0^*} = -P^T \int_{-\infty}^{\log T} w(\log \theta) \left( \log \frac{T}{\theta} \right) d \log \theta \quad (7)$$

The right-hand side of the formula and RED<sup>T</sup> relate to the tube diameter  $D_s$  and to the expansion property. Of course, any frequency can be used for the viscosity; here we use zero

states due to their usage in formulas. A simpler characteristic formula can be obtained using the characteristic temperature  $T_c$ , whose optimal value is at the midpoint of the used and modelled temperatures. Characteristic temperature value  $P_c^T$  is used as described above:

$$\log \frac{\eta_0^*(T)}{\eta_0^*} = -P_c^T \log \frac{T}{T_c} \int_{-\infty}^{\log T} w(\log \theta) d \log \theta \quad (8)$$

RED<sup>T</sup>  $w(\log T)$  can be found by solving the above formula for  $w(\log T)$  as we have derived in previous studies:

$$w(\log T) = -\frac{d}{d \log T} \frac{1}{P_c^T} \frac{\log \frac{\eta_0^*(T)}{\eta_0^*}}{\log \frac{T}{T_c}} \quad (9)$$

The model previously developed using control theory (see Part II, Eq. (3) [2]) for complex viscosity  $\eta^*(\omega)$  can be written also in short exponent form  $\eta^*(\omega) = \eta_0^* e^{-P(\omega)}$ , as can Eq. (7) as  $\eta_0^*(T) = \eta_0^* e^{-P^T(T)}$ , where  $P^T(T) = P^T \int_{-\infty}^{\log T} w(\log \theta) \left( \log \frac{T}{\theta} \right) d \log \theta$ . Thus, we can obtain the complete analytical model by substituting for complex viscosity as a function of frequency and temperature:

$$\eta^*(\omega, T) = \eta_0^* e^{-P(\omega) - P^T(T)} \quad (10)$$

The respective characteristic formula for complex viscosity can be written as

$$\eta^*(\omega, T) = \eta_0^* \log \frac{\omega}{\omega_c} \log \frac{T}{T_c} e^{-P_c(\omega) - P_c^T(T)} \quad (11)$$

In a similar manner we can write a temperature-dependent formula for the characteristic relaxation modulus:

$$G_c(t, T) = G_0 \log \frac{t}{t_c} \log \frac{T}{T_c} e^{-P_c(t) - P_c^T(T)} \quad (12)$$

For shear viscosity we have characteristic formula

$$\eta_c(\dot{\gamma}, T) = \eta_0 \log \frac{\dot{\gamma}}{\dot{\gamma}_c} \log \frac{T}{T_c} e^{-P_c(\dot{\gamma}) - P_c^T(T)} \quad (13)$$

The above equations can also be connected to analytical polymer-structure functions  $P(t)$ ,  $P(\omega)$  and  $P(\dot{\gamma})$ , used instead of analytical temperature function  $P^T(T)$ , and even used with a mixture of these functions due to the presence of linearity.

### 2.3. Time–temperature superposition

The presented principle can be used to explain TTS and modifications thereof. All the relaxation phenomena involved in  $G(t)$  have same temperature dependency, and hence changing the temperature of a measurement will have the same effect on the data as shifting the data horizontally on the log(time) or log(frequency) axis [19]. A very recent paper by Dealy and Plazek [25] reports on the practical use of TTS and milestones, which includes a clear description of where TTS holds and fails. We therefore refer to their analysis and use the same nomenclature (e.g. horizontal shift factor  $a_T$  and vertical shift factor  $b_T$ ). Thus we can write that complex viscosity, which involves both stress and time, requires the application of both shift factors. The master curve is constructed by means of a log–log plot of

$$\frac{b_T}{a_T} \eta^*(T) \text{ versus } \omega a_T.$$

We can explain TTS in a similar manner to Cox-Merz rules starting from the MWD and using melt calibration by converting viscoelastic data between different deformation modes and temperatures:

$$w(M) = \langle |\eta^*(T)|_{\eta^*(T_0), P(T), P^T}; |\eta(T)|_{\eta(T_0), P(T), P^T}; |G(T)|_{G(T_0), P(T), P^T} \rangle \quad (14)$$

where  $P(T) = P' + P''$  as a function of temperature as indicated in Eqs. (2) and (4). The same constant (MWD  $w(M)$ ) in Eq. (14) is used as the starting and reference point this time only for frequency in Fig. 3 and for different REDs and temperatures. As explained above, RED  $w(\log \omega, T)$  is not temperature sensitive, and in practical applications does not exert a significant

effect. Since TTS uses linear operators  $a_T$  and  $b_T$  in a log–log plot and control theory on linear scales, we can write the following approximation for each scale:

$$\eta^*(\omega, T) = \eta_0^* e^{-P(\omega) - P^T(T)} \cong \frac{b_T}{a_T} \eta^*(T) \text{ versus } \omega a_T \quad (15)$$

The vertical ( $b_T$ ) and horizontal ( $a_T$ ) shift factors have empirical or semi-empirical models as for the Arrhenius and WLF equations, or they can be determined directly from the variation with temperature. Master curves can be used to describe the viscoelasticity of linear polymers over a broad range of times, frequencies or shear rates. Eq. (15) explains the use of both a single shift factor and both shift factors simultaneously for thermorheologically simple materials, which has many practical applications for TTS. Analysing TTS and Eq. (15) from the standpoint of control theory reveals that there can be equivalence if the MWD (and especially RED) has the symmetric form of a normalized Gaussian or similar smooth distribution. However, differences appear with more complex distributions, such as a bimodal one.

In a similar way, blends of different polymers or polymers with LCB can be thermorheologically complex, but in most cases they can still be modelled using the control theory principle of wide scales at different temperatures. Moreover, the generated wide master curves violate the presented control theory principle where they join at different temperatures, as obtained in practise when importing master-curve data into the RheoPower software package [2]. We therefore recently added a new module to the software that uses data measured simultaneously at different temperatures without any post-treatment for computation, and generates several best-fit wide master curves at different temperatures.

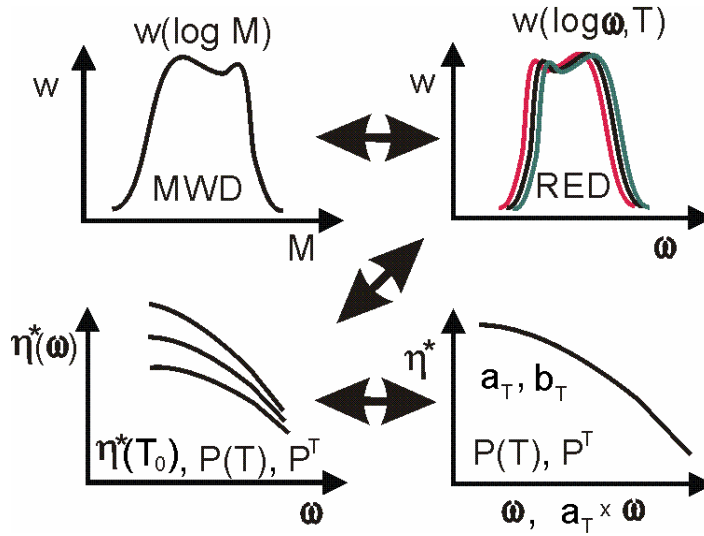


**Figure 3.** Analyses at different frequencies using the presented method of melt calibration yield the MWD that remains the same for different temperatures. TTS holds if the vertical ( $b_T$ ) and horizontal ( $a_T$ ) shift factors give the same viscosity functions as  $P(T)$  and  $P^T$ . In this case we have a thermorheologically rather simple material, and we can obtain by eye the same master curve (i.e. without visible differences) in the lower-right log–log plot.

### 3. Experimental

#### 3.1. Procedure, test polymers and constants

The viscoelasticity and temperature dependence with chain dynamics was modelled. The measured complex viscosity was simulated as a function of frequency and also at a constant frequency as a function of temperature using control theory. The results are compared here with those obtained using Arrhenius and WLF equations. Finally, we discuss more generally used principles, hypotheses, and structures of models and formulas.

Complex viscosity simulations were performed using an analytical model of control theory [2] on a standard PC with the commercial RheoPower software package, and other

simulations were performed using the experimental version of the RheoAnalyzer program of the RheoPower family of software.

The used polymer was Lupolen 1840H LDPE measured at temperatures from 130°C to 250°C as in previous studies. The oscillation rheometer data indicated that  $Mf = 37,800$  g/mol and  $Hf = 2.05$ . The average molecular weight  $M_w = 235,000$  g/mol and  $M_w/M_n = 14.1$  were used. The used sampling band for the analytical model was  $T = 100,000/s$ .

The values of  $P'$  and  $P''$  obtained from the viscosity fitting procedure are listed in Table 1, and no *ad hoc* constants or values were used. A constant characteristic temperature of  $T_c = 190^\circ\text{C}$  was used. The main characteristics of the samples are listed in Table 1.

TABLE 1. Main characteristics of all computations.  $1/P'$  and  $1/P''$  values are not linearly related.

$T$ (°C) <sup>a</sup>	$1/P'$ <sup>b</sup>	$1/P''$ <sup>b</sup>	$P'+P''$ <sup>c</sup>	$R$ <sup>c</sup>	$\eta_0^{*d}$	%RMSE <sup>e</sup>
130	6.56	0.08	13.31	1,122,018	566,867	0.2480
140	1.64	0.09	12.10	1,122,018	357,525	0.4415
150	1.53	0.09	11.84	1,000,000	239,109	0.3548
160	0.93	0.10	10.79	891,251	137,602	0.4790
170	0.76	0.11	10.13	891,251	93,747	0.5107
180	0.60	0.13	9.40	794,328	54,081	0.5455
190	0.51	0.15	8.48	794,328	35,967	0.6087
200	0.47	0.16	8.51	707,946	23,885	0.5714
210	0.43	0.17	8.10	630,957	17,523	0.5759
220	0.39	0.20	7.52	630,957	12,056	0.5345
230	0.37	0.22	7.17	562,341	9,128	0.5436

240	0.34	0.27	6.60	562,341	6,283	0.6194
250	0.32	0.29	6.62	501,187	4,647	0.5493

<sup>a</sup>Temperature.

<sup>b</sup>Obtained elasticity  $P'$  and  $P''$  viscosity values.

<sup>c</sup>Sum of  $P'$  and  $P''$ .

<sup>d</sup>Distance  $R$  set for the ratio of effective distribution ranges.

<sup>e</sup>Obtained percentage root-mean-square error function.

### 3.2. Temperature dependence of viscosity by a model of chain dynamics

Temperature dependences of viscosity are presented in different ways. As a starting point, complex viscosity  $\eta^*$  as obtained using an analytical model [2] is shown in Fig. 3; we previously presented only simulations obtained using a characteristic model of the same measurements. Table 1 indicates that the percentage root-mean-square error function  $\%RMSE$  was 100 times higher than that for the respective characteristic model, but was still less than that for any other model of viscosity. Making the sampling band for the analytical model  $T=1,000/s$  instead of  $T = 100,000/s$  (as used here) would reduce  $\%RMSE$  by more than 50%, but we wanted to use as wide a sampling band as it is reasonable in order to maximize the applicability of the analytical model. Another reason for the higher error is our use of the MWD and RED obtained using the characteristic model, and it appears that the conversion factor between  $M$  and  $\omega$  scales ( $Hf = 2.05$ ) is too small for polyolefin based on calibrations with GPC/SEC measurements. However, this discrepancy does not visibly influence the viscosity or  $P'$  and  $P''$  values, which is the focus of this study. Moreover, solving distribution  $w'(\omega)$  or functions with a logarithmic

kernel is known to be a severely ill-posed problem. A separate study is needed to clarify this matter and to use brute-force computing to obtain  $w'(\log \omega)$  and the MWD using an analytical model at different temperatures.

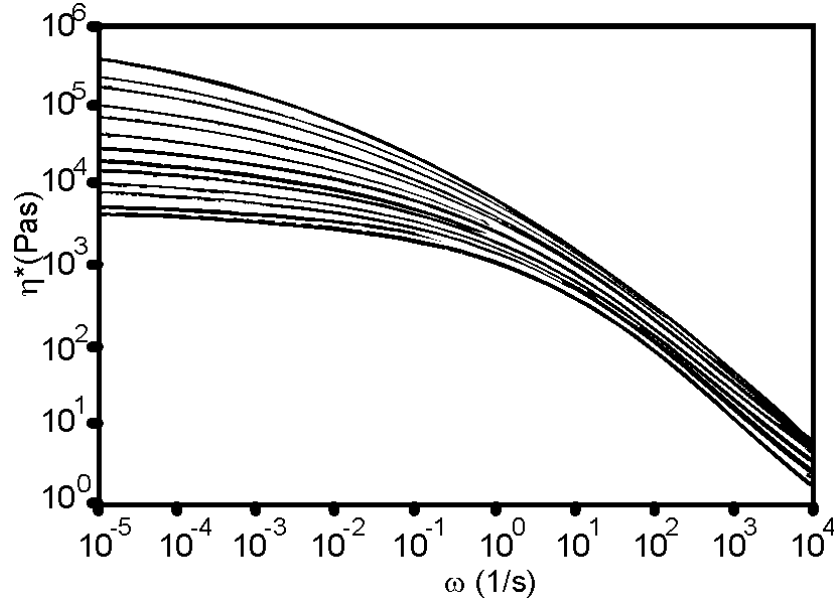


**Figure 3.** Complex viscosity  $\eta^*$  modelled using analytical models for Lupolen 1840H LDPE at temperatures ranging from 130°C (top curve) to 250°C (bottom curve) in 10°C increments. In Part II [2] we modelled the characteristic complex viscosity for the same measurements.

We used the obtained elasticity  $P'$  and  $P''$  viscosity values to study chain dynamics. Fig. 4 indicate that  $P'$  and  $P''$  behave very linearly as a function of temperature and according to formulas for chain dynamics (Eqs. (3) and (4)).

We selected a tube diameter  $D_s = 3.6$  nm [26] and a statistical segment length  $L_s = 50$  nm as it is in range 8 nm-60 nm [19, 27, 28], but accurate absolute values were not essential in this study. Using our values we obtained a friction coefficient of  $\zeta = 10.8 \cdot 10^{-10}$  kg/s at 150°C using Eq. 6. The available literature suggests that  $\zeta = 2.3 \cdot 10^{-10}$  kg/s and density 785kg/m<sup>3</sup> [26], which yields a critical limit complex viscosity of  $\eta_{\infty}^* = 1.26$  Pa s, which is the same as that modelled at

$\omega = 100,000/\text{s}$  in Fig. 3. From this value it is easy to obtain the complete viscosity flow curve for all types of polyethylene if the MWD,  $P'$  and  $P''$  are known.

Using simple linear modelling we obtained  $k' = 4.71$  (elastic scaling factor) and  $a'_T = 0.0016/^\circ\text{C}$  (temperature coefficient) with Eq. (3), and  $k'' = 3.95$  (viscous scaling factor) and  $a''_T = -0.0021/^\circ\text{C}$  (temperature coefficient) with Eq. (4). Similar linear behaviour was found with the characteristic model, with the  $P'$  and  $P''$  values only being lower:  $k' = 24.8$ ,  $a'_T = 0.0245/^\circ\text{C}$ ,  $k'' = 104$  and  $a''_T = -0.080/^\circ\text{C}$ , as shown in Fig. 4. This linear behaviour confirms the validity of the linear model obtained using control theory for chain dynamics also as a function of temperature.

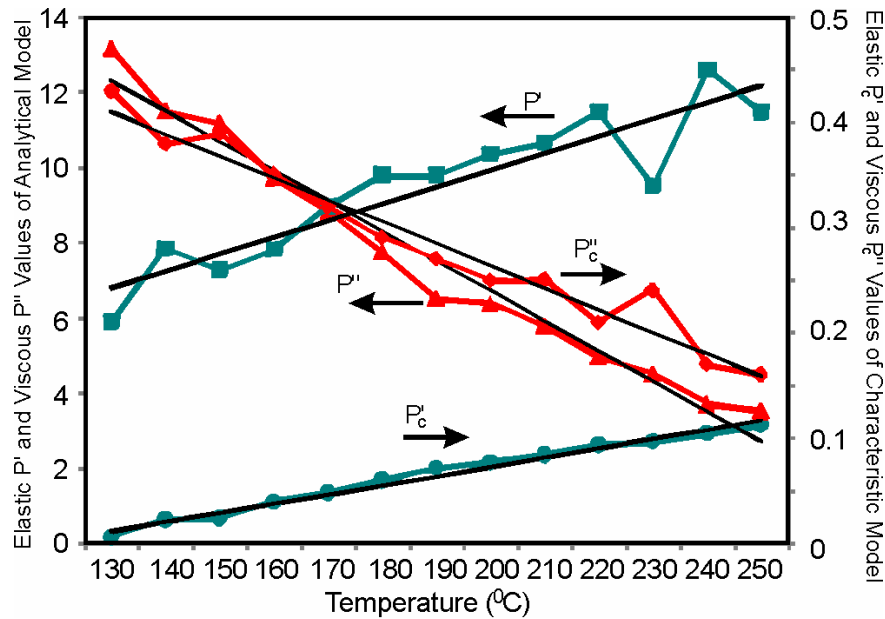


**Figure 4.** Elasticity  $P'$  and viscous  $P''$  values obtained by modelling viscosity  $\eta^*$  with an analytical model (left scale) and a characteristic model (right scale) at different temperatures. Small measurement errors were found for the model at 230°C. Black straight lines are regression fits.

### 3.3. Comparison of temperature dependence by different models

The results obtained using our new method based on control theory were compared with those obtained using Arrhenius and WLF equations. For the control-theory model we used experimental modes of the RheoAnalyzer program and an Excel spreadsheet for the preprocessing of the temperature data scale. We used the characteristic mode and a formula that included viscosity component  $P_c''^T(T)$  as a computation aid:

$$\log \frac{\eta_0^*(T)}{\eta_0^*} = -P_c^T \log \frac{T}{T_c} \int_{-\infty}^{\log T} w(\log \theta) d \log \theta - P_c''^T \log \frac{T}{T_c} \int_{-\infty}^{\log T} w(\log \theta / R) d \log \theta \quad (16)$$

where the “viscous” component with  $P_c''^T$  constant aids the numerical computation when deriving the RED<sup>T</sup> by solving for  $w(\log T)$ , as also done in our previous studies. The formula is written for complex zero viscosity  $\eta_0^*$ , but can be used for any constant frequency, shear rate or relaxation time. It should be noted that the presented RED<sup>T</sup>s are tentative results obtained with an experimental mode of the program, and some coding work is needed to obtain more accurate results.

For the Arrhenius equation we used the standard formula shown in Eq. (17), and for the WLF equation we used Eq. (18), where we use vertical shift factor  $b_T$  instead of the normally used  $a_T$ :

$$b_T = \exp \left[ \frac{E_a}{R} \left( \frac{1}{T} - \frac{1}{T_0} \right) \right] \quad (17)$$

$$b_T = \frac{-c_1^0(T-T_0)}{c_2^0+T-T_0} \quad (18)$$

Data for zero viscosity  $\eta_0^*(T)$  were modelled using an analytical model and taking the data shown in Fig. 3. Note that the data for the Arrhenius and WLF equations were generated directly from these equations, whereas those for the control-theory model required preprocessing in an Excel spreadsheet generating some errors to feed data. Applying a standard best-fit routine yielded  $E_a = 73.5$  kJ/mol for the activation energy, and empirical fitting parameters yielded  $c_1^0 =$

6.95 and  $c_2^0 = 309$  K for zero viscosities.  $R$  in the WLF equation is the universal gas constant.

We get results shown in Fig. 5.

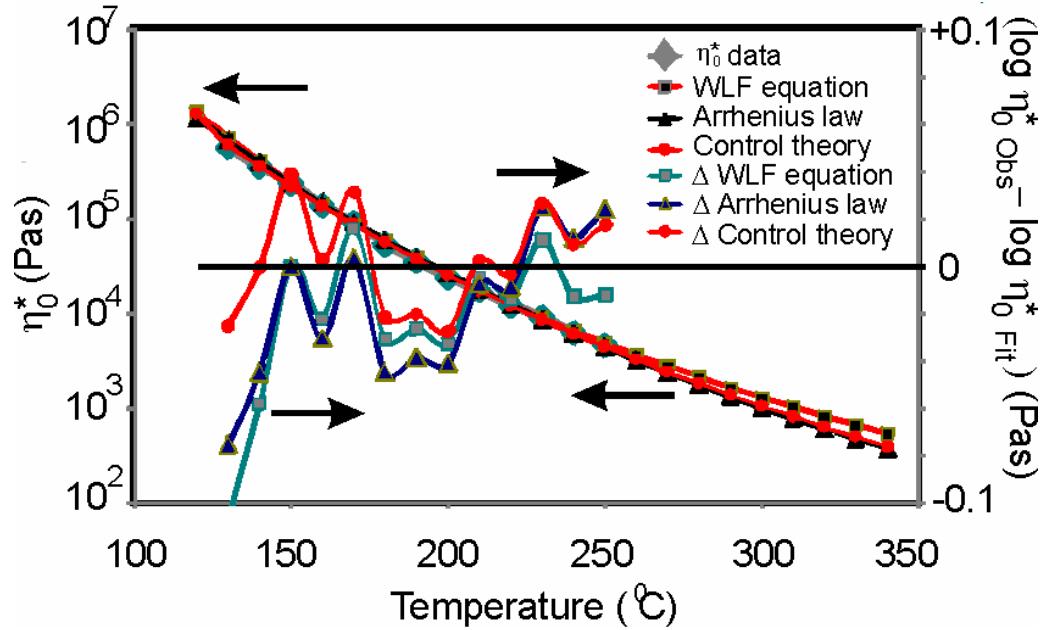


**Figure 5.** Zero viscosity  $\eta_0^*(T)$  data obtained from the analytical model shown in Fig. 3 as a function of frequency, and compared as a function of temperature with the results obtained using the Arrhenius and WLF equations, and control theory.  $\eta_0^*(T)$  modelled using control theory is four times more accurate.

Viscosity  $\eta^*(T)$  was also modelled at  $\omega = 1/s$  as a function of temperature using control theory and the Arrhenius and WLF equations. This yielded  $E_a = 21.0$  kJ/mol,  $c_1^0 = 1.2$  and  $c_2^0 = 220$  K. Modelling using control theory was found to be four times more accurate by  $\%RMSE$  compared to the Arrhenius equations and six times better than with the WLF equation, although some absolute measurement errors were found that were possibly due to the edge effects of polymer melt sample. An oscillation rheometer is known to be a relatively accurate device for frequency-sweep measurements, but differences can appear in the absolute values obtained for

different sample sets of measurement runs. Since we only modelled zero relaxation modulus  $G_0$  generated by zero viscosity, there was sense in making comparisons for  $G_0$ .

### 3.4. Rheologically effective distribution for temperature $w(\log T)$

We computed the  $\text{RED}^T$  function using the Arrhenius and WLF equations, and control theory, and first solved Eq. (16) for distribution  $w(\log T)$  using a similar principle to that described previously [1,2]:

$$w(\log T) = -\frac{d}{d \log T} \frac{1}{P_c^T} \left( \frac{\log \frac{\eta_0^*(T)}{\eta_0^*}}{\log \frac{T}{T_c}} + P_c^{T'} \int_{-\infty}^{\log T} w \left( \log \frac{\theta}{R} \right) d \log \theta \right) \quad (19)$$

Now we can compute limited  $\text{RED}^T$ s, since these distributions tend to widen below 100°C and above 350°C, which are not physically possible for a melt. Thus, we obtained  $\text{RED}^T$ s from curves generated using Arrhenius and WLF equations, and control theory at a frequency of 1/s. The distributions were derived directly from Arrhenius and WLF equations for viscosity  $\eta^*(T)$ . Viscosity data  $\eta^*(T, 1/s)$  were taken from Fig. 3, developed by an analytical model, and the results are shown in Fig. 6.

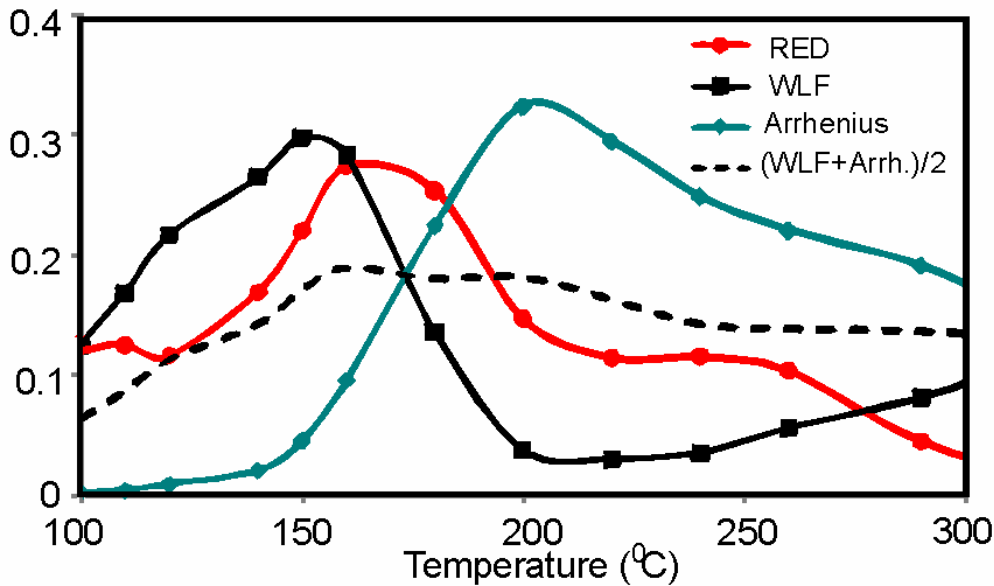


**Figure 6.** Modelled RED<sup>T</sup>s for viscosity  $\eta^*(T)$  at a frequency of 1/s as functions of temperature obtained using the characteristic model.

The physical background of our thermorheology method is principally based on tube expansion according to chain dynamics in a similar way to the elastic and viscous components and values of internal friction coefficient. The RED<sup>T</sup> is derived from the tube expansion rate as a function of temperature. In other words, absolute viscoelastic values as a function of temperature are integral to the RED<sup>T</sup>. Moreover the tube diameter has linear relation to temperature and related to Brownian energy.

### 3.5. RED<sup>T</sup>s as functions of temperature and frequency

Obtaining the three-dimensional RED<sup>T</sup>s as functions of temperature and frequency can provide more useful information, and are generally known as hyphenated techniques. The main data of these samples are listed in Table 2, which includes measured  $\eta^*(T, \omega)$  data. The physical meaning of the abstract nature of zero viscosity  $\eta_0^*(T, \omega)$  for different temperatures at a constant frequency is not yet clear.

TABLE 2. Main characteristics of temperature-sweep computations for different frequencies.

$\omega^a$	$\eta_0^*(T, \omega)^b$	$P_c^T{}^c$	$P_c''^T{}^c$	$P_c^T + P_c''^T{}^c$	$R^d$	%RMSE <sup>e</sup>
0.01	33,771	0.077	0.445	0.522	125	0.1132
0.02	29,432	0.079	0.422	0.501	124	0.1057
0.03	25,339	0.077	0.400	0.477	125	0.0943
0.04	21,487	0.073	0.379	0.452	114	0.0861

0.06	17,960	0.069	0.359	0.428	113	0.0771
0.10	14,816	0.064	0.340	0.405	113	0.0711
0.16	12,068	0.059	0.323	0.383	113	0.0666
0.25	9,713	0.055	0.307	0.362	113	0.0634
0.40	7,727	0.049	0.292	0.341	115	0.0634
0.63	6,083	0.045	0.277	0.322	114	0.0622
1.00	4,752	0.041	0.264	0.305	113	0.0613
1.58	3,675	0.038	0.251	0.289	113	0.0604
2.51	2,820	0.034	0.239	0.273	113	0.0615
3.98	2,149	0.032	0.227	0.260	113	0.0584
6.31	1,626	0.029	0.217	0.246	113	0.0601
10.00	1,222	0.026	0.207	0.232	114	0.0602

<sup>a</sup>Temperature.

<sup>b</sup>Zero viscosity  $\eta_0^*(T, \omega)$  for different temperatures at constant frequency.

<sup>c</sup>Obtained temperature values for  $P^T$  and  $P^{mT}$ .

<sup>d</sup>Distance  $R$  aiding the numerical computation of the distribution (in °C).

<sup>e</sup>Obtained percentage root-mean-square error function.

The generated three-dimensional plot of  $RED^T$  curves in Fig. 7 shows that temperature influences the distributions, with another bump being evident around 270°C. The physical meaning of the bump is not yet clear, but may have something to do with minor additional chain freedoms and tube diameter.

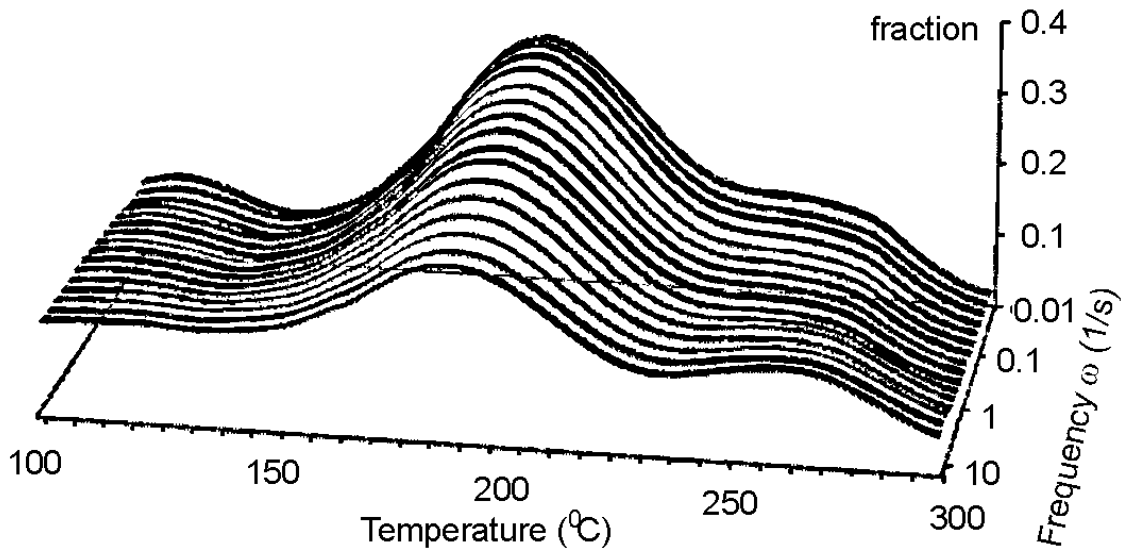


**Figure 7.** Computed three-dimensional family of  $RED^T w(\log T, \omega)$  curves for various temperatures and frequencies. This type of chart can give more structural information, and is generally known as hyphenated techniques. We can obtain that at higher frequencies fewer changes to the tube diameter are needed at different temperatures.

### 3.6. Principles, hypotheses and structures of models and formulas used in the series of linear viscoelastic models (Parts I–IV)

We now summarize more generally the models and formulas for different flows described in these four manuscripts, which are referred simply as Part I to Part IV. The used hypotheses are derived from fundamental principles of molecular dynamics and structure in Parts I and II by statistical procedures with explicit formulas.

In Part I we showed that logarithmic convolution derived from control theory is a linear operation, since it is commutative, associative and distributive. All the formulas presented in Parts I–IV are linear and explicit, but Part II also uses standard and implicit numerical methods

in practise to derive RED  $w(\omega)_{\text{obs}}$ . Similarly, in Part III the complete computation system of orientation simulations using finite element modelling is an implicit procedure.

A new form of the Boltzmann superposition principle used in Part III and the parallel arrangement of forces led to the novel idea of using time-rate separability for transient viscosity and for the relaxation function. The physical model for chains starts from well-known fundamentals and the novel (but still logically presented) melt calibration in Part I and II, with the influences of chains discussed in more detail here (i.e. Part IV). All other hypotheses presented in Parts I–IV and the use of linear and explicit formulas, control theory, and the derivation of RED from data form seamless causal correlations with obtained measurements. In other words, correlations with viscoelastic measurements involved three variables being conducted (the RED function and elasticity  $P'$  and viscous  $P''$  values), where the RED can be converted even to the bimodal MWD or more complicated forms. This manuscript describes how  $P'$  and  $P''$  exhibit linear behaviour relating to chain dynamics and dimensions. In short, we obtained stable statistical correlations and viscoelastic fits simultaneously.

*Ill-posed inverse problems* are discussed for Part II, which in this case tend towards a well-posed state. Most attempts in the field have led to integral equations, which are known to be ill-posed. Inverse problems usually do not fulfil Hadamard's postulates of *well-posedness*; namely, they might not have a solution in the strict sense, or the solutions might not be unique and/or might not depend continuously on the data. Since  $w(\omega)_{\text{obs}}$  is computed directly by derivation from measured data using a characteristic model and is converted into relative fractions of the MWD  $w(M)$ , this segment curve fulfils the definition of well-posedness. In contrast, the analytical model used to obtain the MWD is highly ill-posed.

Part II yields some information from the difference viscosity curve  $\Delta\eta^* = \eta^*_{obs} - \eta^*_{fit}$ , and from the direction of %RMSE convergence to develop  $w(\omega)_{fit}$  side curves. Thus, these out-of-range regions are still mildly ill-posed.

The wide  $\eta^*_{fit}$  and  $G(t)$  fulfil the well-posedness definition, even though the curves are based on a form of extrapolation (actually in the linear model) that works in all directions. If the model is highly consistent with measurements—within the range of numerical round-offs—it can be expected to provide accurate estimations of new data outside the measured data range.

In contrast, although the temperature-dependency model correlates empirically well with measurements according to mathematical treatments similar to those presented above, chain models and the origin of certain behaviours are partially affected by temperature-dependent viscoelasticity.

#### **4. Conclusions**

This study has connected chain dynamics to the different viscoelastic properties up to the macro scale in a linear manner. The modelling method applied in the study started from simpler oriented chain topologies using elementary physics for chain elastic and viscous forces, and connected these to control-theory models for the relaxation modulus, dynamic and shear viscosities governed by the RED, and the melt calibration governed by the MWD. The temperature dependence of viscoelasticity was used to explain chain dynamics and tube dimensions. This paper provides a foundation for future studies of more complicated chain dynamics found in close relaxed states as reptation, primitive path fluctuations, constraint release, and other entangled and disentangled chain dynamics.

Another important feature of the four papers for linear viscoelastic models (i.e. the present paper plus [1–3]) other than multiscale modelling is the inclusion of well-described hypotheses and the use of explicit formulas.

Control theory was successfully used to model the temperature dependence of viscoelasticity, with the results being much more accurate than those obtained using semi-empirical Arrhenius or WLF equations. Viscoelastic values at different temperatures are related to the RED and are also a function of temperature  $RED^T$ . The tube diameter is linearly related to temperature, which is related to Brownian energy. TTS and master curves are therefore verified for thermorheologically simple materials.

The demonstrated properties represent only a small proportion of the additional different applications for viscoelasticity and material analyses obtainable from control theory.

A future possible development of these linear viscoelastic models is a novel type of measurement routines for the same polymer according to standardized instructions.

## **Acknowledgements**

We thank many scientists for fruitful discussions and the referees of this series of papers for their constructive criticisms.

## **References**

- [1] T. Borg, E. J. Pääkkönen, Linear viscoelastic models: Part I. Relaxation modulus and melt calibration, *J. Non-Newtonian Fluid Mech.* 156 (2009) 121–128.
- [2] T. Borg, E. J. Pääkkönen, Linear viscoelastic models: Part II. Recovery of the molecular weight distribution using viscosity data, *J. Non-Newtonian Fluid Mech.* 156 (2009) 129–138.

- [3] T. Borg, E. J. Pääkkönen, Linear viscoelastic models: Part III. Start-up and transient flow effects from the molecular weight distribution, *J. Non-Newtonian Fluid Mech.* 159 (2009) 17–25.
- [4] R. B. Bird, C. F. Curtiss, R. C. Armstrong and O. Hassanger (1987). *Dynamics of Polymeric Liquids*, Vol. 2. Kinetic Theory, 2nd Ed., New York: John Wiley & Sons. New York.
- [5] M. van Gurp, J. Palmen J, Time-temperature superposition for polymeric blends, *Rheol Bulletin* 67 (1998) 5–8.
- [6] P. Wood-Adams, S. Costeaux, Thermorheological effects of long-chain branching in entangled polymer melts, *Macromol.* 34 (2001) 6281–6290.
- [7] W. W. Graessley, V. R. Raju, Some rheological properties of solutions and blends of hydrogenated polybutadiene, *J. Poly. Sci.: Poly. Symp.* 71 (1984) 77–93.
- [8] D. J. Lohse, S. T. Milner, L. J. Fetters, M. Xenidou, N. Hadjichristidis, R. A. Mendelson, C. A. Garcia-Franco, M. K. Lyon, Well-defined, model long chain brached polyethylene. Melt rheological behavior, *Macromolecules* 35 (2002) 3066–3075.
- [9] P. H. P. Macaubas, N. R. Demarquette, Time-temperature superposition principle applicability for blends formed of immiscible polymers, *Polymer Engineering and Science*, 42 (2002) 1509–1519.
- [10] M. Giamberini, V. Ambrogi, P. Cerruti, C. Carfagna, Viscoelasticity of main chain liquid crystalline elastomers, *Polymer* 47 (2006) 4490–4496.
- [11] C. Kagarise, K. W. Koelling, Y. Wang, S. E. Bechtel, A unified model for polystyrene–nanorod and polystyrene–nanoplatelet melt composites, *Rheol Acta* 47 (2008) 1061–1076.
- [12] J. Kim, D. H. Kim and Y. Son, Abnormal Rheological Behavior of Linear Low Density Polyethylene Melts at High Shear Rate, *Polymer Bulletin* 60 (2008) 821–828.

- [13] H. C. Öttinger, M. Laso, Smart polymers in finite-element calculations, in Theoretical and applied rheology, P. Moldenaers and R. Keunings (Eds.), Vol. 1, Proc. XIth Int. Congr. on Rheology, Elsevier, Amsterdam (1992) 286–288.
- [14] M. Laso, H. C. Öttinger, Calculation of viscoelastic flow using molecular models: the CONNFESSIT approach, *J. Non-Newtonian Fluid Mech.*, 47 (1993) 1–20.
- [15] H. C. Öttinger, Stochastic processes in polymeric fluids: tools and examples for developing simulation algorithms, Springer, Berlin, 1996.
- [16] R. Keunings, Micro-macro methods for the multiscale simulation of viscoelastic flow using molecular models of kinetic theory, in: D.M. Binding, K. Walters (Eds.), *Rheology Reviews 2004*, British Society of Rheology (2004) 67–98.
- [17] C. C. Hua, J. D. Schieber, Nonequilibrium Brownian dynamics of Hookean and FENE dumbbells with internal viscosity, *J. Non-Newtonian Fluid Mech.* 56 (1995) 307–332.
- [18] G. K. Batchelor, *An Introduction to Fluid Mechanics*, Cambridge University Press, Cambridge, UK, 1967.
- [19] J. M. Dealy, R. G. Larson, *Structure and Rheology of Molten Polymers, From Structure to Flow Behavior and Back Again*, Carl Hanser Verlag, Munich, 2006.
- [20] M. J. Struglinski, W. W. Graessley, Effects of polydispersity on the linear viscoelastic properties of entangled polymers. 1. Experimental observations for binary mixtures of linear polybutadiene, *Macromolecules* 18 (1985) 2630–2643.
- [21] H. Mavridis, R. Shroff, Appraisal of a Molecular Weight Distribution-to-rheology conversion scheme for linear polyethylenes, *J. of Appl. Poly. Sci.*, 49 (1993) 299–318.
- [22] C. Pattamaprom, R. G. Larson, T. J. Van Dyke, Quantitative predictions of linear viscoelastic rheological properties of entangled polymers, *Rheol. Acta* 39 (2000) 517–531.

- [23] C. Pattamaprom, R. G. Larson, Predicting the linear viscoelastic properties of monodisperse and polydisperse polystyrenes and polyethylenes, *Rheol. Acta* 40 (2001) 516–532.
- [24] E. van Ruymbeke, R. Keunings, C. Bailly, Determination of the molecular weight distribution of entangled linear polymers from linear viscoelasticity data, *J. Non-Newtonian Fluid Mech.* 105 (2002) 153–175.
- [26] J. Dealy, D. Plazek, Time-Temperature Superposition – A Users Guide, *Rheol Bulletin* 78(2) (2009) 16–31.
- [26] L. J. Fetters, D. J. Lohse, H. R. Colby. Chain dimensions and entanglement spacing. In *Physical Properties of Polymers Handbook*. 2nd edit. (2006) E. J. Mark, Ed. Springer, New York.
- [27] W. W. Graessley, *Polymeric Liquids and Networks: Dynamics and Rheology*, Garland Science, London, 2008.
- [28] J. D. Ferry, *Viscoelastic properties of polymers*, Wiley, New York, 1980, p. 330.